SPC

Advanced Journal of Chemistry-Section A

Journal homepage: www.ajchem-a.com

Original Research Article

α-Fe_2O_3 Nanoparticles: Synthesis, Characterization, Magnetic Properties and Photocatalytic Degradation of Methyl Orange

Aliakbar Dehno Khalaji[1]*, Pavel Machek[2], Marketa Jarosova[2]

[1] *Department of Chemistry, Faculty of Science, Golestan University, Gorgan, Iran*

[2] *Institute of Physic of the Czech Academy of Sciences, Na Slovance 2, 182 21 Prague, Czech Republic*

ARTICLE INFO

Article history

Submitted: 27 June 2021
Revised: 20 July 2021
Accepted: 05 August 2021
Available online: 07 August 2021
Manuscript ID: AJCA-2106-1268

DOI: 10.22034/AJCA.2021.292396.1268

KEYWORDS

α-Fe_2O_3
Magnetic nanoparticles
Photocatalyst
Degradation

ABSTRACT

α-Fe_2O_3 magnetic nanoparticles (MNPs) (Fe-1, Fe-2 and Fe-3) were prepared by a simple wet chemical precipitation route and characterized by Fourier transform infrared spectroscopy (FT-IR), X-ray diffraction (XRD) and transmission electron microscopy (TEM). The magnetic behaviors of the as-prepared Fe_3O_4 nanoparticles were done using vibrating sample magnetometer (VSM). In addition, the as-prepared α-Fe_2O_3 nanoparticles were used as photocatalyst for degradation and removal of methyl orange (MO) dye under visible light irradiation from aqueous solution. The influence of various parameters such as contact time and dosage of catalyst have been examined and discussed. The studies revealed that the degradation of MO reached to 95% (Fe-1), 88% (Fe-2) and 62% (Fe-3) within 120 min by increasing of catalyst dosage from 0.02 g to 0.06 g. Degradation rates of MO by Fe-1, Fe-2 and Fe-3 were 0.0249, 0.0177 and 0.0081 min^{-1}, respectively, indicating that the degradation depends on the crystalline size and morphology of the α-Fe_2O_3 magnetic nanoparticles.

GRAPHICAL ABSTRACT

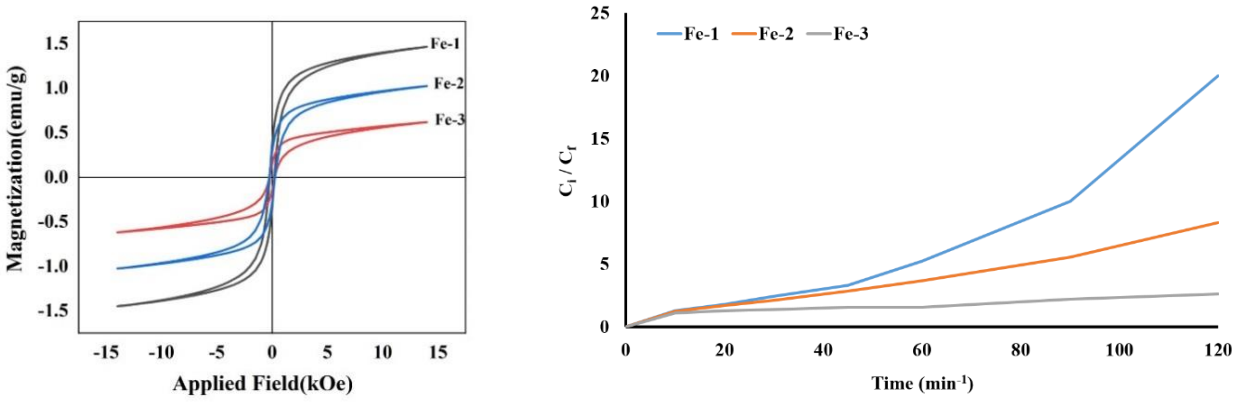

* Corresponding author: Dehno Khalaji, Aliakbar
✉ E-mail: alidkhalaji@yahoo.com

Introduction

Hematite, as an eco-friendly nanoparticles and as an n-type semiconductor with a band gap of 2-2.2 eV, is one of the most stable transition metal oxide, inexpensive and stable in aqueous solution (pH > 3) and it has various good properties and applications [1-5]. In addition, it has a great potential as adsorbent to remove of various dyes and metal ions from aqueous solution [1, 2, 7-16]. In 2019, Qiu *et al*. reported photocatalytic degradation of rhodamine B using hollow polyhedral α-Fe_2O_3 in water under visible light irradiation [1]. Debanth *et al.* [8] synthesized α-Fe_2O_3 by simple chemical precipitation as adsorbent for removal of methyl orange dye. At the optimum condition, more than 90% methyl orange removal was achieved. Saha *et al*. reported effective adsorption of different dyes on iron oxide (α-Fe_2O_3) nanoparticles [9]. Results of Saha and co-workers represented that the functional groups of organic dyes are important parameter to the removal of them by iron oxide nanoparticles. Ye *et al*. [10] synthesized the rhombohedral α-Fe_2O_3 using one-step controllable process and reported that about 91% of bisphenol A was degraded under the simulated sunlight irradiation. A great amount of effort has been focused to improve the photocatalytic performance of organic dyes using α-Fe_2O_3 nanoparticles [10-14]. Gandha *et al.* [11] reported the mesoporous iron oxide nanowires to removal of methylene blue, rhodamine B and methyl orange dyes, using 90 min irradiation. Wang *et al*. [12] studied photodegradation of the methyl orange by mesoporous magnetic Fe_2O_3 nanoparticles under visible light irradiation. Moreover, another various nanoparticles for photocatalytic degradation of methyl orange such as Au/TiO_2 [16], Ag/TiO_2/biochar composite [17], TiO_2 [18], ZnO [18], graphene oxide [18] and magnetically retrievable supported ionic liquid phase [19] have been reported until now. Morphology of the α-Fe_2O_3 nanoparticles may affect their physical and chemical properties [8-14]. Various techniques and several iron precursor used to the preparation of different shapes of α-Fe_2O_3 nanoparticles [20-25].

Recently, we prepared α-Fe_2O_3 nanoparticles with various shapes using solid state thermal decomposition of various iron precursors [20, 21, 24, 25]. In this research study, α-Fe_2O_3 nanoparticles were prepared using a simple wet chemical precipitation route at the presence of various ratio (w/w) of iron precursors and polyvinyl alcohol (PVA) and then calcined at 600 °C for 3 h under air atmosphere. The α-Fe_2O_3 nanoparticles were characterized by FT-IR, XRD, TEM and VSM. In addition, the photodegradation of methyl orange has been studied under visible light irradiation.

Experimental

Materials

All materials used in this paper are of analytical grade and were purchased from Aldrich and Merck companies. They were used without any further purification.

Characterization

FT-IR spectra were recorded using a KBr disk by FT-IR Perkin-Elmer spectrophotometer. XRD patterns of α-Fe_2O_3 nanoparticles were recorded on Empyrean powder diffractometer of PANalytical in Bragg-Brentano configuration equipped with a flat sample holder and PIXCel3D detector (Cu Kα radiation, λ = 1.5418 Å). TEM images were recorded with a transmission electron microscope (TEM) FEI Tecnai G^2 20 with a LaB_6 cathode at acceleration voltage 200 kV. The instrument is equipped with a CCD camera Olympus Veleta. The magnetic properties of α-Fe_2O_3 nanoparticles were recorded by the vibrating sample magnetometer (VSM) with a sensitivity of 5 × 10^6 emu.

Synthesis of α-Fe_2O_3 nanoparticles

Nanoparticles Fe-1 were prepared by a simple wet chemical precipitation route. 10 mL aqueous solution of $FeCl_3 \cdot 6H_2O$ (1 g) and 1 g PVA were mixed and stirred for about 30 min. Then, a solution of NaOH (0.1 M) was added drop by drop to the above solution until pH reached 11. After 3 h stirred, the red-brown precipitates were prepared, which is symbolic of formation of α-Fe_2O_3. The precipitates were filtered, washed, dried and calcined at 600 °C for 3 h. In analogous procedure, the Fe-2 and Fe-3 nanoparticles were prepared using 1 g of $Fe(NO_3)_3$ and $Fe_2(SO_4)_3$, respectively.

Photodegradation

Photodegradation of MO by the as-prepared α-Fe_2O_3 nanoparticles was tested using a 300 W Xe-lamp with a 420 nm cutoff filter as a visible light source. Various amounts of α-Fe_2O_3 nanoparticles (0.02, 0.04 and 0.06 g) were added to a 50 mL of aqueous MO solution (35 ppm) and stirred at the speed of 250 rpm in the dark (30 min) to establish the adsorption equilibrium. Then, the mixture was irradiated by Xe-lamp and after 15 min intervals 2 mL of mixture was withdrawn, the catalyst was centrifuged at 1500 rpm. The concentration of MO were detected by UV-Vis spectrophotometer at λ_{max} = 473 nm. All the experiment were performed at room temperature.

Results and Discussion

FT-IR spectra

Figure 1 presents the FT-IR spectra of the as synthesized α-Fe_2O_3 nanoparticles. A peak that appears at 574 cm^{-1} was assigned to the vibration of Fe-O bond [1, 8, 14, 15, 26], which can be observed in all three samples. The peaks that appear at 1000-1700 cm^{-1} were corresponded to the vibrations of C-H and C-O groups of PVA [27-29]. Finally, the peaks that correspond to the vibration of O-H bonds of PVA or water molecules adsorbed on the surface of the as-prepared α-Fe_2O_3 nanoparticles appeared at about 1600 and 3450 cm^{-1} [27-29].

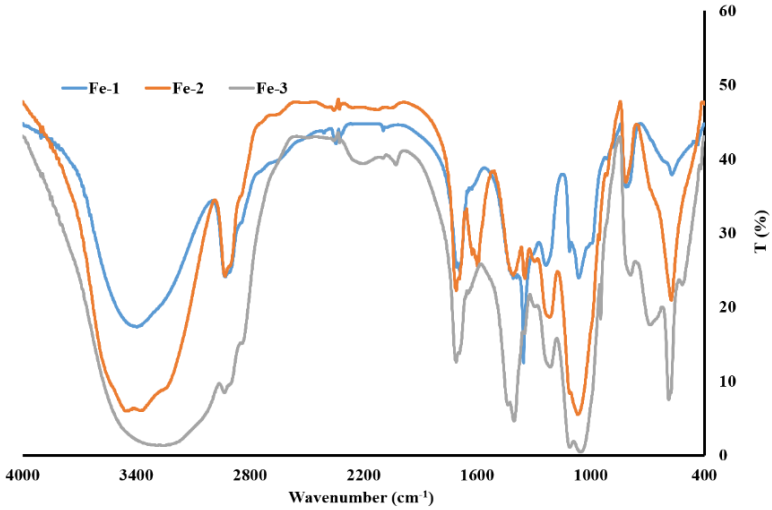

Figure 1. FT-IR spectra of the as-prepared Fe-1, Fe-2 and Fe-3 nanoparticles

XRD patterns

XRD patterns of α-Fe_2O_3 nanoparticles are represented in Figure 2. The sharp diffraction peaks at 2θ ≈ 24.14°(012), 33.15°(104), 35.62°(110), 40.85°(113), 49.45°(024), 54.06°(116), 57.59°(018), 62.43°(214), 63.99°(300), 71.93°(1010) and 75.44°(220) can

be well assigned to the rhombohedral phase of α-Fe_2O_3 [20-25]. Rietveld fit in crystallographic program Jana 2006 confirmed the structure [30] and determined the lattice constants a=5.0357 Å and c=13.7513 for sample Fe-1 and very similar values for samples Fe-2 and Fe-3. Whereas samples Fe-1 and Fe-2 seem to be pure, sample Fe-3 contains still a small amount of the precursor $Fe_2(SO_4)_3$ which is well documented by its most intensive peak (113) at 24.73° in the diffraction pattern.

The sizes of crystallites were calculated using fundamental parameter approach [31]. The instrumental function was modeled from the known geometry of the diffractometer and from the predefined radiation profiles. The instrumental broadening β_{sample} was subsequently extracted from the measured diffraction pattern and sample broadening β_{sample} was determined. Average crystallite sizes were then solved using Scherrer equations as shown in Equation (1).

$$D_v = K\lambda / (\beta_{sample} \cos\theta) \quad (1)$$

Where D_v is volume weighted crystallite size, K is Scherrer constant, λ wavelength of the radiation and β_{sample} is integral breadth of reflection located at angle 2θ.

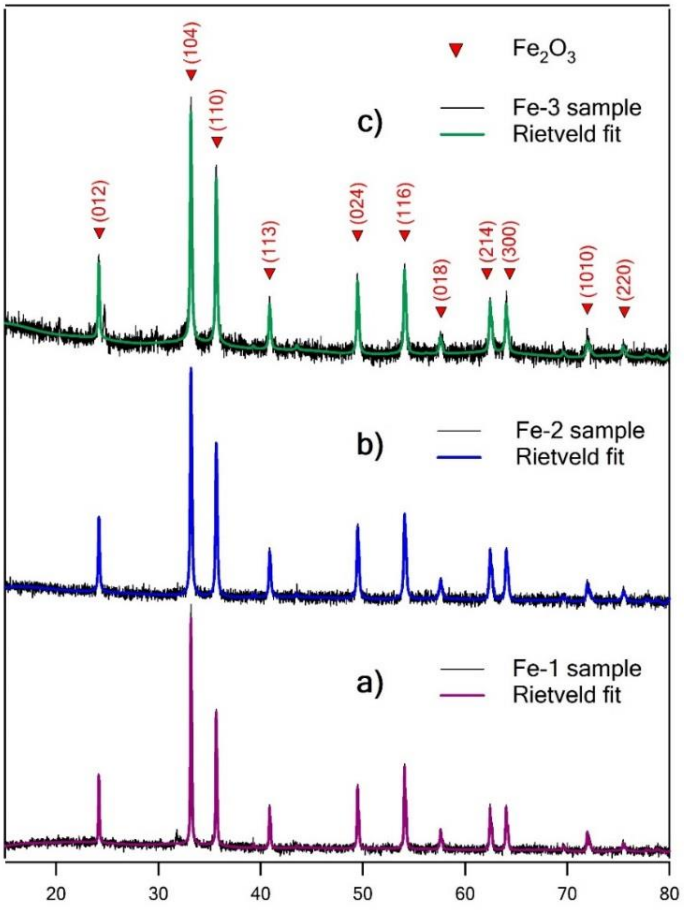

Figure 2. XRD patterns of a) Fe-1, b) Fe-2 and c) Fe-3 nanoparticles

The calculated average crystallite sizes are 99.0 nm, 62.8 nm and 60.4 nm for Fe-1, Fe-2 and Fe-3, respectively. These results are close to the values seen in the TEM images (Figure 4). The smaller size of catalyst increases the interaction and

degradation of MG onto the surface of the as-prepared α-Fe_2O_3 nanoparticles [8].

TEM analysis

The morphology of the as-prepared α-Fe_2O_3 nanoparticles was investigated by TEM (Figure 3). The shape of nanoparticles is rectangle for Fe-1, ellipsoid for Fe-2 and irregular for Fe-3. Particle sizes are about 80-100 nm for Fe-1 and about 50 nm for Fe-2 and Fe-3. The TEM images confirm that the α-Fe_2O_3 nanoparticles sizes and shapes depend largely on the iron precursor used.

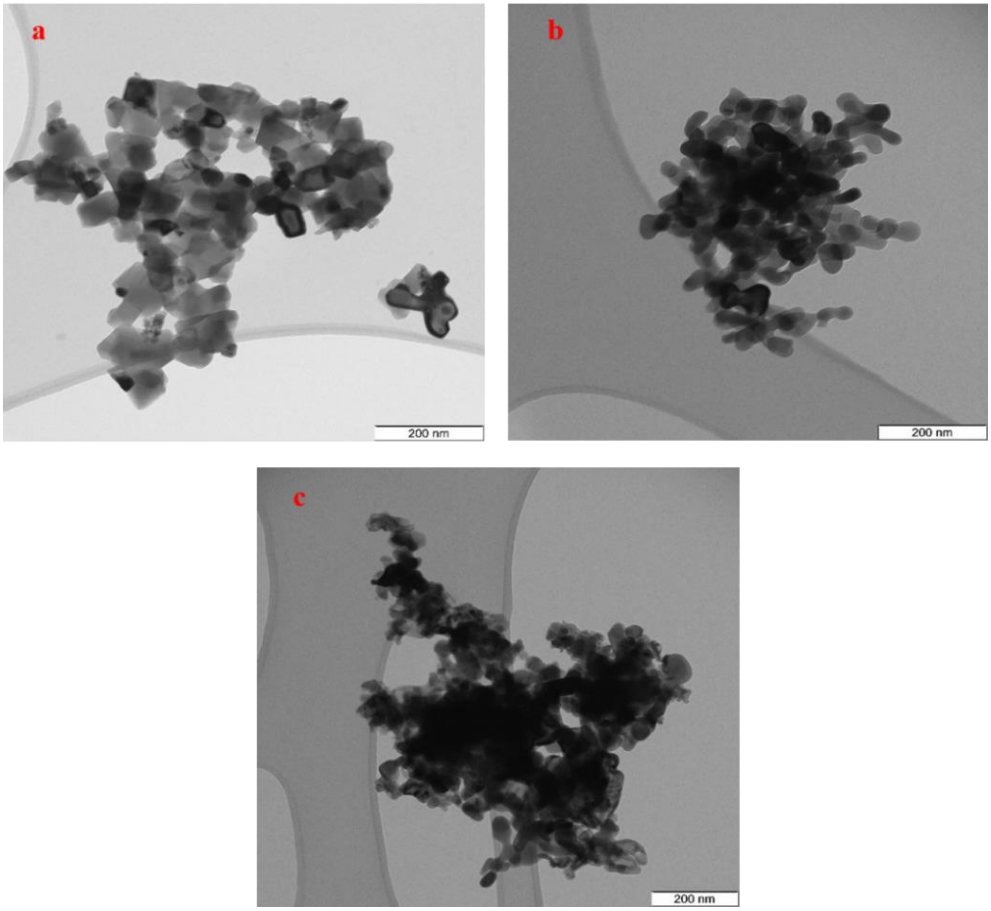

Figure 3. TEM images of a) Fe-1, b) Fe-2 and c) Fe-3 nanoparticles

Magnetic characteristics

Magnetic properties of α-Fe_2O_3 nanoparticles were investigated at room temperature by a vibrating sample magnetometer (VSM) using applying the 15000 Oe magnetic field [23]. The magnetic hysteresis curves are shown in Figure 4. This figure reveals that the products exhibit paramagnetic behavior [11] and that the magnetic saturation (Ms) were about 1.5, 1 and 0.6 emu/g for Fe-1, Fe-2 and Fe-3, respectively. It can be seen that the saturation magnetization of Fe-1 > Fe-2 > Fe-3. On the contrary to the observation of Lassoued *et al*. [22], the decrease in the value of Ms is here assigned to the decrease in the particle size. This result confirmed that the magnetic properties of the as-synthesized α-Fe_2O_3 nanoparticles depend on the synthetic method, particle size and morphology [22, 23].

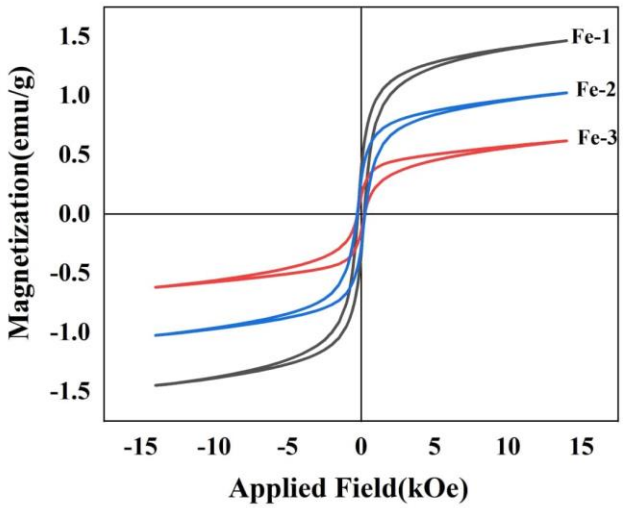

Figure 4. Hysteresis loops of a) Fe-1, b) Fe-2 and c) Fe-3 nanoparticles

Photocatalytic activity

Hematite (α-Fe_2O_3) nanoparticles with band gap ≈ 2.1 eV are a good material to absorb visible light and to perform as photocatalyst to speed up degradation of various organic dyes from aqueous solution such as bisphenol A [10], rhodamine B [1,13], congo red [14] and methyl orange [11,12]. Studies on the degradation of methyl orange show that in the absence of catalyst there is no change at the maximum adsorption wavelength of methyl orange under visible light irradiation [12]. In the presence of catalyst, the degradation speed of methyl orange depends on the dosage of catalyst, contact time, light irradiation and pH [11,12,16-19]. The percentage of MO degradation was calculated using the following Equation (2).

$$D\% = \{(C_i - C_f) \times 100\} / C_i \quad (2)$$

where C_i and C_f are initial and final concentration (mg/L), respectively.

The effect of various dosages of the as-prepared α-Fe_2O_3 nanoparticles on the MO degradation at different contact times is depicted in Figure 5. All the experiment were performed at initial concentration of 35 ppm for methyl orange. As can be seen in Figure 5, increased dosage of the photocatalyst from 0.02 to 0.06 g enhanced the photo-degradation efficiency from 65% to 95% for Fe-1, from 57% to 88% for Fe-2 and from 42% to 62% for Fe-3. The reason was that the increase of active sites of catalyst enhanced the interaction between the surface of catalyst and the surface of methyl orange dye [11, 12, 17, 19].

Figure 6 illustrates the degradation curves of methyl orange at the presence of Fe-1, Fe-2 and Fe-3. The rate constant for Fe-1 is higher than Fe-2 and Fe-3 due to the different the particle size and morphology of the catalyst [12] and also the different electrostatic between surface charge of nanocatalyst and methyl orange [11]. As seen in Figure 6, at similar condition, the photocatalytic activity of Fe-1 > Fe-2 > Fe-3.

The degradation results show that the photocatalytic reaction fits a pseudo-first-order dependency [11,12,16,19] and the rate constant k (min^{-1}) can be calculated from the following Equation 3.

$$Ln (C_i / C_f) = kt \quad (3)$$

The fitting curves of photodegradation reaction of methyl orange are basically linear and are

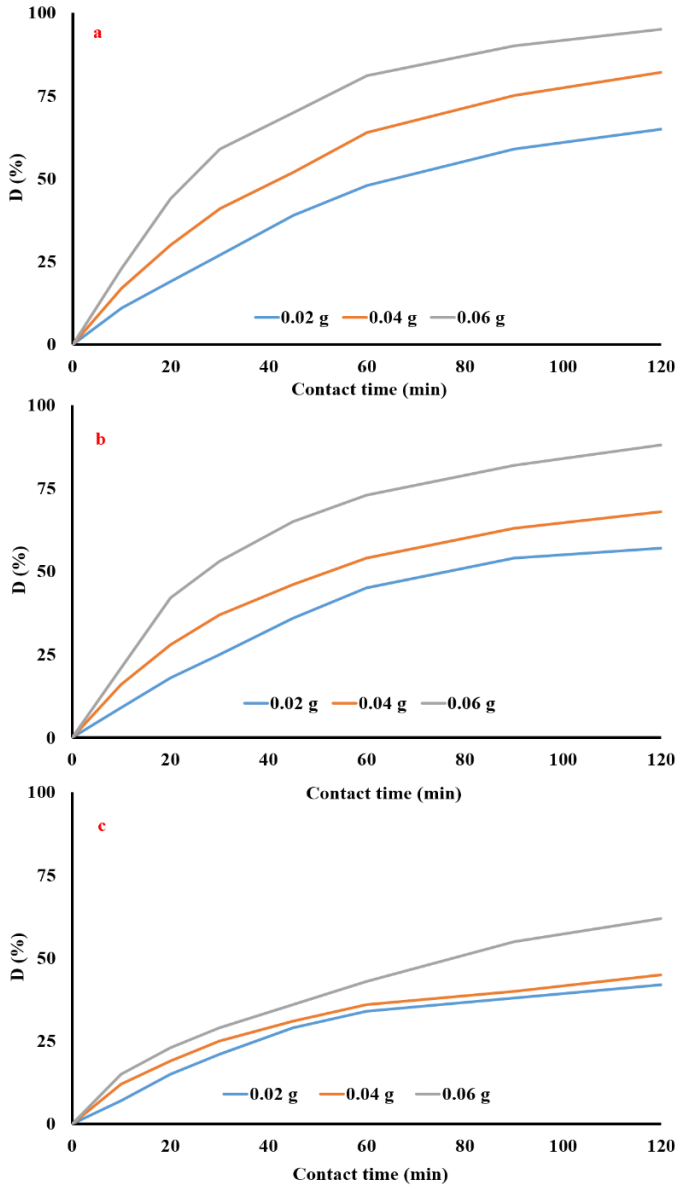

Figure 5. The effect of dosage of a) Fe-1, b) Fe-2 and c) Fe-3 nanoparticles and contact time on the photodegradation percentage (D%) of MO

presented in Figure 7. From the slope of the curves, the rate constant k value was determined to be 0.0249, 0.0177 and 0.0081 min^{-1} for Fe-1, Fe-2 and Fe-3, respectively. The k for Fe-1 and Fe-2 values are 3.07 and 2.18 times larger than the k for Fe-3. These results indicate that the photodegradation of methyl orange depends on the crystallite size and morphology of the as prepared α-Fe_2O_3 nanoparticles. The rate constant *k* of Fe-1, Fe-2 and Fe-3 is higher than that of the mesoporous magnetic Fe_2O_3 nanoparticles (*k* = 0.0056 – 0.0057 min^{-1}) [12], but lower than that of Fe_2O_3/ZnO (*k* = 0.052 min^{-1}) [11].

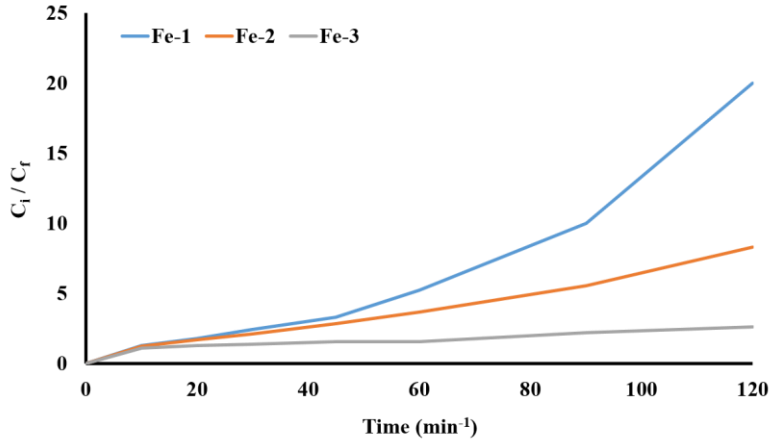

Figure 6. Photodegradation of MO as function of contact time (catalyst dosage is 0.06 g)

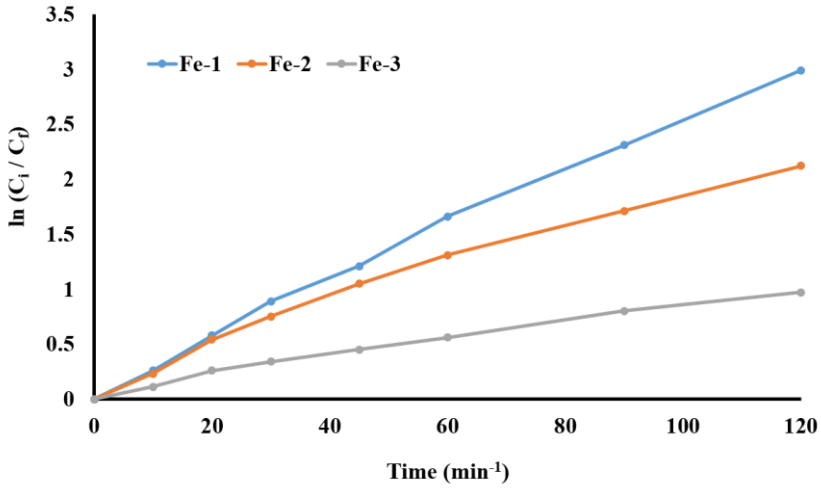

Figure 7. Kinetic curves of photodegradation of MO (catalyst dosage is 0.06 g)

Conclusions

In this work, three α-Fe_2O_3 magnetic nanoparticles (Fe-1, Fe-2 and Fe-3) were successfully synthesized using a simple wet chemical precipitation route, and the material was characterized using the FT-IR, XRD and TEM. Magnetic measurements revealed ferromagnetic properties of the nanoparticles and low level of magnetic saturation. Photocatalytic degradation of MO by these α-Fe_2O_3 magnetic nanoparticles revealed that the degradation of MO reached 95% (Fe-1), 88% (Fe-2) and 62% (Fe-3). Degradation rate of MO by Fe-1, Fe-2 and Fe-3 were 0.0249, 0.0177 and 0.0081 min^{-1}, respectively, indicating that the degradation depended on the crystalline size and morphology of the α-Fe_2O_3 magnetic nanoparticles.

Acknowledgements

We would like to thank the Golestan University and Institute of Physic of the Czech Academy of Sciences for financial their supports. The work is supported by Operational Programme Research, Development and Education financed by European Structural and Investment Funds and the Czech Ministry of Education, Youth and Sports (Project No. SOLID21 CZ.02.1.01/0.0/0.0/16_019/0000760).

Disclosure statement

No potential conflict of interest was reported by the authors.

ORCID

Aliakbar D. Khalaji: 0000-0002-1787-2951

References

[1] M. Qiu, R. Wang, X. Qi, *J. Tiwan Inst. Chem. Eng*., **2019**, *102*, 394–402. [CrossRef], [Google Scholar], [Publisher]

[2] C. Tamez, R. Hernandez, J.G. Parsons, *Microchem. J*., **2016**, *125*, 97–104. [CrossRef], [Google Scholar], [Publisher]

[3] Y. Al-Douri, N. Amrane, M.R. Johan, *J. Mater. Res. Technol.*, **2019**, *8*, 2164–2169. [CrossRef], [Google Scholar], [Publisher]

[4] G. Rahman, Z. Najaf, A. ul Haq Ali Shah, S.A. Mian, *Optik,* **2020**, *200*, 163454. [CrossRef], [Google Scholar], [Publisher]

[5] Z. Li, Y. Mao, Q. Tian, W. Zhang, L. Yang, *J. Alloys Compd.*, **2019**, *784*, 125–133. [CrossRef], [Google Scholar], [Publisher]

[6] H.J. Shiply, K.E. Engagtes, V.A. Grover, *Environ. Sci. Pollut. Res*., **2013**, *20*, 1727–1736. [CrossRef], [Google Scholar], [Publisher]

[7] T. Shahriai, N. Mehrdadi, M. Tahmasebi, *Pollution*, **2019**, *5*, 515–524. [CrossRef], [Google Scholar], [Publisher]

[8] A. Debnath, K. Deb, K.K. Chattopadjyay, B. Saha, *Desal. Water treat*., **2016**, *57*, 13549–13560. [CrossRef], [Google Scholar], [Publisher]

[9] B. Saha, S. Das, J. Saikia, G. Das, *J. Phys. Chem. C*., **2011**, *115*, 8024–8033. [CrossRef], [Google Scholar], [Publisher]

[10] C. Ye, K. Hu, Z. Niu, Y. Lu, L. Zhang, K. Yan, , *J. Water Process* Eng., **2019**, *27*, 205–210. [CrossRef], [Google Scholar], [Publisher]

[11] K. Gandha, J. Mohapatra, M. Kabir Hossain, K. Elkins, N. Poudyal, K. Rajeshwar, J.P. Liu, *RSC Adv*., **2016**, *6*, 90537–90546. [CrossRef], [Google Scholar], [Publisher]

[12] J. Wang, X. Shao, Q. Zhang, G. Tian, X. Ji, W. Bao, *J. Mol. Liq*., **2017**, *248*, 13–18. [CrossRef], [Google Scholar], [Publisher]

[13] A. Kusior, K. Michalec, P. Jelen, M. Radecka, *Appl. Surf. Sci*., **2019**, *476*, 342–352. [CrossRef], [Google Scholar], [Publisher]

[14] S. Taghavi Fardood, F. Moradnia, S. Moradi, R. Forootan, F. Yekke Zare, M. Heidari, *Nanochem. Res*., **2019**, *4*, 140–147. [CrossRef], [Google Scholar], [Publisher]

[15] D.M.S.N. Dissanayale, M.M.M.G.P.G. Mantilaka, T.C. Palihawadana, G.T.D. Chandrakumara, R.T. De Silva, H.M.T.G.A. Pitawala, K.M. Nalin de Silva, G.A.H. Amaratunga, *RSC Adv*., **2019**, *9*, 21249–21257. [CrossRef], [Google Scholar], [Publisher]

[16] M. Tsuji, K. Matsuda, M. Tanaka, S. Kuboyama, K. Uto, N. Wada, H. Kawazumi, T. Tsuji, H. Agi, J.I. Hayashi, *ChemistrySelect,* **2018**, *3*, 1432–1438. [CrossRef], [Google Scholar], [Publisher]

[17] R. Shan, L. Lu, J. Gu, Y. Zhang, H. Tuan, Y. Chen, B. Luo, *Mater. Sci. Semiconduct. Process*., **2020**, *114*, 105088. [CrossRef], [Google Scholar], [Publisher]

[18] R. Raliya, C. Avery, S. Chakrabarti, P. Biswas, *Appl. Nanosci*., **2017**, *7*, 253–259. [CrossRef], [Google Scholar], [Publisher]

[19] A.G. Naikwade, M.B. Jagadale, D.P. Kale, A.D. Gophane, K.M. Garadkar, G.S. Rashinkar, *ACS Omega*, **2020**, *5*, 131–144. [CrossRef], [Google Scholar], [Publisher]

[20] A.D. Khalaji, S.M. Mousavi, M. Jarosova, P. Machek, *J. Synch. Investig.*, **2020**, *14*, 1191–1194. [CrossRef], [Google Scholar], [Publisher]

[21] A.D. Khalaji, M. Ghorbani, *Chem. Methodol*., **2020**, *4*, 532–542. [CrossRef], [Google Scholar], [Publisher]

[22] A. Lassoued, M.S. Lassoued, B. Dkhil, A. Ammar, A. Gadri, *Physica E: Low Dimens. Syst. Nanostruct.*, **2018**, *101*, 212–219. [CrossRef], [Google Scholar], [Publisher]

[23] S. Sharma, N. Dhiman, A. Kumar, M. Singh, P. Dhiman, *Integr. Ferroelectr.*, **2020**, *204*, 38–46. [CrossRef], [Google Scholar], [Publisher]

[24] A.D. Khalaji, Z. Palang Sangdevini, S. Mousavi, M. Jarosova, P. Machek, *Asian J. Nanosci. Mater.*, **2021**, *4*, 137–146. [CrossRef], [Google Scholar], [Publisher]

[25] A.D. Khalaji, S. Mousavi, Z. Palang Sangdevini, M. Jarosova, P. Machek, M. Dusek, *J. Sci. Islam. Repub. Iran,* **2021,** *32*, 201. [CrossRef], [Google Scholar], [Publisher]

[26] A.M. Mazrouaa, M.G. Mohamed, M. Fekry, *Egypt. J. Petrol.*, **2019**, *28*, 165–171. [CrossRef], [Google Scholar], [Publisher]

[27] P.K. Khanna, N. Singh, S. Charan, V.V.V.S. subbarao, R. Gokhale, U.P. Mulik, *Mater. Chem. Phys.*, **2005**, *93*, 117–121. [CrossRef], [Google Scholar], [Publisher]

[28] N.K. Subramani, S.K. Nagaraj, S. Shivanna, H. Siddaramaiah, *Macromolecules,* **2016**, *49*, 2791–2801. [CrossRef], [Google Scholar], [Publisher]

[29] K. Zhou, S. Jiang, C. Bao, L. Song, B. Wang, G. Tang, Y. Hu, Z. Gui, *RSC Adv.*, **2012**, *2*, 11695–11703. [CrossRef], [Google Scholar], [Publisher]

[30] V. Petricek, M. Dusek, L. Palatinus, *Z. Kristallogr.*, **2014**, *229*, 345–352. [CrossRef], [Google Scholar], [Publisher]

[31] R.W. Cheary, A.A. Coelho, *J. Appl. Cryst.*, **1998**, *31*, 862–868. [CrossRef], [Google Scholar], [Publisher]

HOW TO CITE THIS ARTICLE

Aliakbar Dehno Khalaji*, Pavel Machek, Marketa Jarosova. α-Fe_2O_3 Nanoparticles: Synthesis, Characterization, Magnetic Properties and Photocatalytic Degradation of Methyl Orange. *Adv. J. Chem. A*, **2021**, 4(4), 317-326.

DOI: 10.22034/AJCA.2021.292396.1268
URL: http://www.ajchem-a.com/article_134768.html